Available online at www.sciencedirect.com

ScienceDirect

IFAC Papers Online CONFERENCE PAPER ARCHIVE

IFAC PapersOnLine 58-20 (2024) 464–469

Underwater vehicle navigation using bearing measurements from a mobile beacon ⋆

Simon A. Hoff * **Henrik M. Schmidt-Didlaukies** *
Erlend A. Basso * **Damiano Varagnolo** * **Kristin Y. Pettersen** *

* *Department of Engineering Cybernetics, Norwegian University of Science and Technology (NTNU), Trondheim, Norway (e-mail: {simon.a.hoff,henrik.schmidt,erlend.a.basso, damiano.varagnolo,kristin.y.pettersen}@ntnu.no).*

Abstract: Autonomous underwater vehicles enable efficient underwater operations such as mapping, surveillance, and inspection. However, due to the lack of global navigation satellite systems (GNSS) signals, drift in pose estimates will occur over time. Common solutions to this issue are using either stationary or mobile beacons to provide range and possibly bearing measurements to bound the navigation error over time. However, this requires occupying communication bandwidth to get reliable round-trip range measurements. In this paper, we propose a system where a mobile beacon passively listens to communications from the underwater vehicle to estimate the position of the vehicle. We show that the estimation error is bounded over time through strategic movement of the mobile beacon.

Keywords: Underwater localization techniques, Communication in marine domain, Maritime robotics

1. INTRODUCTION

The oceans represent a large resource that is still not sufficiently explored and utilized. According to NOAA (2023), only 24.9 % of the seafloor was explored as of 2023. As we increase our activity below the ocean surface and develop new infrastructure, our need for effective means of inspection, surveillance, and maintenance increase accordingly.

Autonomous underwater vehicles (AUVs) can enable such operations to be executed faster and at a lower cost than existing solutions. Most tasks today have to be performed either by Remotely Operated Vehicles (ROVs) or by trained divers, which is expensive and requires large crews to manage operations. Conversely, as AUVs become more capable they may operate for weeks at a time without human intervention.

Navigation of underwater vehicles is still a significant challenge. Due to the strong attenuation of electromagnetic waves in water, underwater vehicles are unable to access positioning systems such as Global Navigation Satellite Systems (GNSS) while submerged. This means that they are generally forced to rely on dead reckoning using inertial measurement units (IMUs) and Doppler velocity logs (DVLs) to estimate their position. This leads to an unbounded increase in localization uncertainty over time (Chitre, 2010).

A common solution to this challenge is the deployment of acoustic beacons to aid the AUVs in localizing themselves. The placement of stationary beacons providing range measurements does, however, suffer from two drawbacks. First, range measurements either depend on round-trip messaging, which can require significant communication bandwidth in multi-agent systems, or require carefully synchronized clocks, which may also require significant bandwidth. Second, the placement of stationary beacons will, in many cases, lead to significant costrelated to the deployment and retrieval of beacons before and after an operation. An alternative approach is to use mobile beacons attached to a support vessel instead. However, this may incur large operating costs if the support vessel is crewed. Autonomous surface vessels (ASVs) may provide a more cost-effective solution for long-term missions.

There have been many contributions to the topic of localization of underwater vehicles with mobile beacons using range measurements. Crasta et al. (2018) explored the observability in underwater target localization using a single autonomous surface vehicle with range measurements. Bayat et al. (2016) demonstrated localizing both an

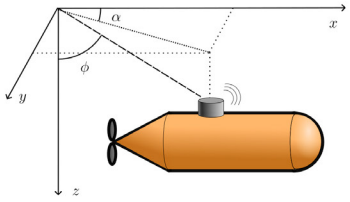

Fig. 1. Overview of the geometry of the USBL bearing measurements. Here, α denotes the azimuth angle, and ϕ denotes the elevation angle.

⋆ This work was supported by the European Research Council (ERC) under the European Union's Horizon 2020 research and innovation programme, through the ERC Advanced Grant 101017697-CRÈME, and by the Research Council of Norway through project No. 302435 and the Centres of Excellence funding scheme, project 223254, NTNU AMOS.

10.1016/j.ifacol.2024.10.097

AUV and an unknown number of stationary beacons simultaneously using only an attitude and heading reference system, as well as range measurements to all beacons. Further, Hung et al. (2022) used multiple surface vehicles to localize an unknown underwater vehicle using range measurements and adaptive motion.

Usually, range measurements with acoustic transmissions are performed using a round-trip range measurement. This has the drawback that additional communication bandwidth must be utilized, and individual measurements must be made for interaction with every agent.

An alternative approach to round-trip range measurements is utilizing synchronized clocks on all agents to measure the message transmission time with one-way messages. Due to clock drift, it is, however, not sufficient to synchronize clocks at the start of a mission, leading to the need for continuously synchronizing the clocks. It is worth noting that with typical underwater sound speeds of around $c = 1500\text{m/s}$, a difference of just 1 ms would lead to an error of 1.5 m in the range measurement. Due to the latency and uncertainty in sound propagation time in underwater systems, it is therefore clear that unless the system is carefully designed and calibrated, and the clock synchronization is carefully designed, errors may be significant. Further, typical state-of-the-art clock synchronization algorithms such as Giridhar and Kumar (2006) or Leng and Wu (2011) are dependent on two-way messaging, which when scaled to $N > 2$ agents lead to significant communication overhead.

Long baseline systems (LBL) utilize multiple range measuring modems spaced far apart to triangulate the position of a modem or pinger using range measurements, as described in Austin et al. (1984). A later development from these systems was the Short Baseline System (SBL). These function with the same principle as the LBL systems, but with much shorter spacing between receivers, typically limited by the physical dimensions of the ship hulls that they would be mounted to.

Ultra-Short Baseline Systems (USBL) further reduce the size of the full system, to the extent where the multiple receivers are combined in an array, and potted as one unit (Austin, 1994; Jaffre et al., 2005). Rather than range measurements, USBL systems utilize the phase difference between the acoustic receivers to estimate the bearing of an incoming signal. This means that USBL systems can measure the bearing without the need for round-trip messaging or synchronized clocks. This enables retrieving some information about the location of the underwater vehicle without the need for the ASV to occupy any communication bandwidth that may be better utilized for other purposes, for instance for inter-agent communication in the case of multiple AUVs cooperating.

In this paper, we propose a system where a mobile beacon mounted on an ASV passively listens to communications from an AUV to estimate the position of the vehicle. This enables utilizing larger parts of the communication bandwidth of the acoustic channel for other purposes than localization, such as planning and coordination. Specifically, we develop and test an algorithm for adaptively moving the ASV and thus the USBL beacon, in order to localize the AUV. By fusing the bearing information from the USBL system with information from the inertial navigation system (INS) in the AUV, we show that the ASV is able to achieve bounded estimation errors over time through strategic movement.

The paper is organized as follows. In Section 2, we introduce the measurement models, AUV estimation model, and filter structure used to localize the AUV with USBL bearing measurements. In Section 3, we propose a planning strategy for the ASV to maximize the information gained in the measurements. In Section 4 we present the vehicle modeling and control algorithms used for simulation. In Section 5 we present the results and discussion, and in Section 6 we present conclusions and future work.

2. AUV LOCALIZATION

In this section, we describe the estimator used by the surface vehicle to determine the position of the underwater vehicle. We first introduce the mechanism to obtain bearing measurements from the USBL system, and then describe how these bearing measurements may be particle-filtered into a position estimate.

2.1 Obtaining bearing measurements from USBL systems

As depicted graphically in Figure 1, a USBL modem will measure the bearing of the incoming signal as the relative azimuth angle α, defined as

$$\alpha\left(\boldsymbol{p}_{\text{AUV}}, \boldsymbol{p}_{\text{ASV}}, \psi_{\text{ASV}}\right) = \arctan_2\left(y_{\text{AUV}} - y_{\text{ASV}}, x_{\text{AUV}} - x_{\text{ASV}}\right) - \psi_{\text{ASV}}, \quad (1)$$

and the elevation angle ϕ, defined as

$$\phi\left(\boldsymbol{p}_{\text{AUV}}, \boldsymbol{p}_{\text{ASV}}\right) = \arccos\left(\frac{z_{\text{AUV}} - z_{\text{ASV}}}{\|\boldsymbol{p}_{\text{AUV}} - \boldsymbol{p}_{\text{ASV}}\|}\right), \quad (2)$$

assuming that the pitch and roll of the ASV are 0. This assumption is usually violated in a practical context, however it is trivial to correct the measurement using the estimated attitude from the ASVs navigation system. If both the error of the navigation system and the measurement error of the bearing measurement are gaussian, then the corrected bearing measurement will be gaussian as well, but with a higher variance. Here $\boldsymbol{p} = [x, y, z]^T$ refers to the position of each vehicle in the NED coordinate frame and ψ is the heading of the vehicle. Based on Tracey (1992); Chan et al. (1978), we assume the measurement noise model for both azimuth and elevation angles to be an additive zero-mean and gaussian noise, with a heteroskedasticity that depends on the distance between the agents. Specifically, if we let $r = \|\boldsymbol{p}_{\text{AUV}} - \boldsymbol{p}_{\text{ASV}}\|$ indicate the distance between the modems, then the gaussian noise associated to azimuth and elevation is modeled to have a variance given by

$$\sigma_\alpha^2(\boldsymbol{p}_{\text{AUV}}, \boldsymbol{p}_{\text{ASV}}) = \sigma_\phi^2(\boldsymbol{p}_{\text{AUV}}, \boldsymbol{p}_{\text{ASV}}) = \left(\frac{\text{rad}}{180^\circ}\pi r\right)^2 \sigma_{\text{USBL}}^2, \quad (3)$$

with σ_{USBL} a baseline standard deviation of the measurement that may be expressed as a percentage of the acoustic range in degrees (Blueprint subsea, 2024).

2.2 Particle filtering the bearing measurements

Particle filters are suitable for estimating state evolutions in cases where one or more system models are nonlinear, or

the process or measurement noise is non-gaussian. While algorithms similar to particle filters have been used since the 1950s, the first use of the term, as well as rigorous proofs of its properties, were introduced by Pierre Del Moral in Moral (1996) and Moral (1998). In this paper, we assume gaussian heteroskedastic noise models, while the state evolution and measurement models are highly nonlinear. This makes a particle filtering approach more suitable for estimating the probability distribution of the AUV position than a nonlinear Kalman filter.

Similar to Jain et al. (2018), we consider a stochastic unicycle model for tracking the AUV, but with additional bias terms for the pitch and yaw angles to estimate the angle rates as approximately constant. We use the variable u to denote the surge speed, ψ the heading, θ the pitch, and b_ψ and b_θ are the forcing terms for the evolutions of the corresponding angles, with time constant T_b. We collect these quantities in the particle state vector $\boldsymbol{x}_i = [x, y, z, \theta, \psi, u, b_\theta, b_\psi]^T$, and model an evolution step $\Delta\boldsymbol{x}_i$ using a truncated gaussian denoted by $\overline{\mathcal{N}}$, to reduce the number of invalid particles after the propagation step

$$\Delta\boldsymbol{x}_i \sim \overline{\mathcal{N}}\left(\begin{bmatrix} u\cos\theta\cos\psi \\ u\cos\theta\sin\psi \\ -u\sin\theta \\ b_\theta \\ b_\psi \\ 0 \\ -\frac{1}{T_b}b_\theta \\ -\frac{1}{T_b}b_\psi \end{bmatrix} \Delta t, \operatorname{diag}\left(\begin{bmatrix} \sigma_x^2 \\ \sigma_y^2 \\ \sigma_z^2 \\ \sigma_\theta^2 \\ \sigma_\psi^2 \\ \sigma_u^2 \\ \sigma_{b_\theta}^2 \\ \sigma_{b_\psi}^2 \end{bmatrix} \Delta t^2\right)\right), \quad (4)$$

with $\sigma_\star$ as the standard deviation of variable $\star$. The distribution is truncated to $z \in [z_1, \infty)$, with z_1 a coefficient larger than zero that reflects that the AUV should avoid the splash zone, $\theta \in [-\pi/2, \pi/2]$, and $u \in [0, \infty)$. We also introduce the variable Δt to denote the time step of the filter, which accounts for changes in the communication frequency. While the filter may still need to be re-tuned for different communication frequencies, this variable simplifies the process.

According to the particle filtering paradigm, we use model (4) to estimate the probability density function (pdf) for the state as a swarm of particles and alternate this prediction step propagating the particles with a measurement-based correction step, where the particles are reweighted according to data from the USBL system.

More precisely, after receiving a USBL message the algorithm first assigns weights $w(\boldsymbol{x}_i)$ to each particle $\boldsymbol{x}_i$, $i \in 1, ..., N_{\text{particles}}$ based on the measurement likelihood function

$$w(\boldsymbol{x}_i) \leftarrow w(\boldsymbol{x}_i) \cdot l(\boldsymbol{x}_i \mid \boldsymbol{y}) \quad (5)$$

with $l(\boldsymbol{x}_i|\boldsymbol{y})$, the likelihood for the state value $\boldsymbol{x}_i$ given the just received measurement $\boldsymbol{y}$.

For the USBL bearing measurement, the likelihood function is given by

$$\begin{aligned} &l(\boldsymbol{x}_i \mid y_{\text{USBL}}) \\ &\quad = \mathcal{N}\left(y_{\text{USBL}} - h_{\text{USBL}}(\boldsymbol{p}_i, \boldsymbol{p}_{\text{ASV}}, \psi_{\text{ASV}}), \begin{bmatrix} \sigma_\alpha & 0 \\ 0 & \sigma_\phi \end{bmatrix}\right), \end{aligned} \quad (6)$$

with σ_α and σ_ϕ given by (3), and

$$h_{\text{USBL}}(\boldsymbol{p}_i, \boldsymbol{p}_{\text{ASV}}, \psi_{\text{ASV}}) = \begin{bmatrix} \alpha(\boldsymbol{p}_i, \boldsymbol{p}_{\text{ASV}}, \psi_{\text{ASV}}) \\ \phi(\boldsymbol{p}_i, \boldsymbol{p}_{\text{ASV}}) \end{bmatrix}, \quad (7)$$

where α and ϕ are given by (1) and (2), respectively, and $\boldsymbol{p}_i = [x_i, y_i, z_i]^T$ denotes the position vector for particle i. These likelihood functions assume that the location of the ASV is exactly known. This is not the case in practice, but with modern high-precision GNSS systems the precision will usually be sufficiently high that the filtering performance should not be significantly affected.

To make use of the information from the AUV's navigation system, we also implement a second measurement vector. In our case, this consists of the vehicle speed, heading, and depth. The reason for this choice is that while reliable measurements may not be available, all of these measurements will tend to have an expected value that is approximately equal to the ground truth (i.e. for practical purposes we may assume the measurement noise to be zero mean). The likelihood corresponding to this part of available information follows then as

$$l(\boldsymbol{x}_i|y_{\text{INS}}) = \mathcal{N}\left(\begin{bmatrix} \psi_{\text{AUV}} \\ U_{\text{AUV}} \\ z_{\text{AUV}} \end{bmatrix}, \begin{bmatrix} \sigma_\psi^2 & 0 & 0 \\ 0 & \sigma_U^2 & 0 \\ 0 & 0 & \sigma_z^2 \end{bmatrix}\right), \quad (8)$$

with ψ being the heading, U the speed over ground, z the depth, and σ_ψ, σ_U, and σ_z the standard deviations for heading, speed, and depth, respectively.

We finally implement periodical particle resampling by picking particles with replacement from the current pool of particles with probability

$$p(\boldsymbol{x}_i) \propto w(\boldsymbol{x}_i), \quad (9)$$

after which all particle weights are reset to be equal to $1/N_{\text{particles}}$.

3. TRAJECTORY OPTIMIZATION

In this section, we propose a method for directing the ASV to maximize the performance of the AUV localization algorithm. First, we propose a metric for evaluating ASV positions, then we describe a method to find the next point to visit based on this performance metric.

To maximize the value of new measurements, we introduce the following method of evaluating the utility of a given position. Consider the estimated pdf of the AUV position $\boldsymbol{p}_{\text{ASV}}$ at time j, $p(\boldsymbol{p}_{\text{ASV}}[j])$. We consider the value added through a USBL measurement at a given location as the covariance of the distribution of measurement deviations from the expectation, normalized for the measurement variance through a Mahalanobis transform

$$\begin{aligned} \boldsymbol{C}_{\boldsymbol{p}_{\text{ASV}}} = \operatorname{Cov}\Bigg(&\begin{bmatrix} \sigma_\alpha^{-2} & 0 \\ 0 & \sigma_\phi^{-2} \end{bmatrix} \Big(h(\boldsymbol{x}_i, \boldsymbol{p}_{\text{ASV}}, \psi_{\text{ASV}}) \\ &- \mathbb{E}_i\left[h(\boldsymbol{x}_i, \boldsymbol{p}_{\text{ASV}}, \psi_{\text{ASV}})\right]\Big)\Bigg) \end{aligned} \quad (10)$$

where h is the USBL measurement function, $\boldsymbol{x}_i$ is the ith particle, and $\mathbb{E}[\cdot]$ is the expectation operator. Multiple alternative ways to measure the added information based on the covariance matrix exist. The most direct way is generalized variance, defined as the determinant of $\boldsymbol{C}_{\boldsymbol{p}_{\text{ASV}}}$ (Wilks, 1932). Alternatively, we may consider the largest direction of variance, also known as the first principal component, namely the largest eigenvalue of $\boldsymbol{C}_{\boldsymbol{p}_{\text{ASV}}}$.

The evaluation method corresponds to constraints on the movement of the surface vessel. By only considering the largest eigenvalue (axis of largest variance), there is less constraint on the motion of the surface vessel, providing more freedom for the next steps.

The planning algorithm is based on the idea of sampling possible locations of the space to find the best next location to visit. Densely sampling the entire NE-plane, even if constrained to some range from the AUV, would lead to excessive computational expense. Thus, it is necessary to find an effective strategy for sampling candidate positions.

The first step is to constrain the sampled positions to an annulus around the belief position for the AUV $\{\boldsymbol{p}_s \text{ s.t. } r_1 < ||\boldsymbol{p}_s - \hat{\boldsymbol{p}}_{\text{AUV}}|| < r_2\}$. By assuming that the particle distribution is symmetric about the axis from the ASV through the mass center of the particle distribution, we know that the evaluation metric will also be approximately symmetric about the axis. This means that we only have to sample one side, which we choose by which side the ASV is currently pointing towards. The points in this "half-annulus" may be expressed by $\boldsymbol{p}_s = \hat{\boldsymbol{p}}_{\text{AUV}} + \boldsymbol{p}_r$, i.e. as the sum of the belief position of the AUV, and a displacement rotated by means of a Rodrigues rotation

$$\boldsymbol{p}_r = \boldsymbol{v}\cos\beta + (\boldsymbol{k}\times\boldsymbol{v})\sin\beta + \boldsymbol{k}(\boldsymbol{k}\cdot\boldsymbol{v})(1-\cos\beta) \quad (11)$$

where $\beta \in [0,\pi]$, the displacement vector $\boldsymbol{v} = r\frac{\boldsymbol{p}_{\text{ASV}}-\boldsymbol{p}_{\text{AUV}}}{\|\boldsymbol{p}_{\text{ASV}}-\boldsymbol{p}_{\text{AUV}}\|}$, with the radius $r \in [r_1, r_2]$, and the axis of rotation

$$\boldsymbol{k} = \frac{\boldsymbol{v}_{\text{ASV}} \times (\hat{\boldsymbol{p}}_{\text{AUV}} - \boldsymbol{p}_{\text{ASV}})}{\|\boldsymbol{v}_{\text{ASV}} \times (\hat{\boldsymbol{p}}_{\text{AUV}} - \boldsymbol{p}_{\text{ASV}})\|}. \quad (12)$$

In addition to reducing computation costs, this also reduces that maximum amount of turning that the ASV will be required to do, reducing the energy expended.

A final challenge arises from the fact that it is not known how long it will take the ASV to reach the target location when sampling. For this paper we handle this issue naively, by assuming a number of steps required for the ASV to reach the next position, and then shift the target position according to the estimated speed and course of the AUV.

As the ASV will require multiple communication cycles to reach the next waypoint $\boldsymbol{p}_W[j]$ (j being the index of the current waypoint), the motion per cycle is handled as follows. We consider the current location $\boldsymbol{p}_a$ as the along-track position of the ASV on the line between the previous waypoint and the next waypoint

$$\boldsymbol{p}_a = \boldsymbol{p}_W[j-1] + \text{proj}_{\boldsymbol{p}_W[j]-\boldsymbol{p}_W[j-1]}(\boldsymbol{p}_{\text{ASV}} - \boldsymbol{p}_W[j-1]), \quad (13)$$

with the projection of vectors $\boldsymbol{a}$ and $\boldsymbol{b}$ is given as

$$\text{proj}_{\boldsymbol{a}}(\boldsymbol{b}) = \frac{\boldsymbol{a}\cdot\boldsymbol{b}}{\|\boldsymbol{a}\|\,\|\boldsymbol{b}\|}\boldsymbol{a}. \quad (14)$$

The target position $\boldsymbol{p}_t$ for the current communication cycle $t \in [t[k-1], t[k]]$, with $t[k] = t[k-1] + \Delta t$ is then set based on a nominal speed for the ASV, which should be set lower than the true maximum speed of the vehicle to account for recovery from across-track errors

$$\boldsymbol{p}_t = \boldsymbol{p}_a + \frac{\boldsymbol{p}_W[j] - \boldsymbol{p}_W[j-1]}{\|\boldsymbol{p}_W[j] - \boldsymbol{p}_W[j-1]\|} u_{\text{nom.}} \Delta t. \quad (15)$$

The next waypoint $\boldsymbol{p}_W[j+1]$ is computed when the ASV is sufficiently close to the current waypoint that it will be reached within the next communication cycle

$$\|\boldsymbol{p}_W[j] - \boldsymbol{p}_{\text{ASV}}\| < u_{\text{nom.}} \Delta t. \quad (16)$$

The guidance system used to follow the resulting series of straight-line paths is described in Section 4.4.

4. SIMULATIONS

In this section, we describe the fundamental modeling and control-theoretical modeling for the vehicles used in this paper, as well as their respective control systems.

4.1 Vehicle Modeling

A general 6-DOF model for a marine vehicle can be stated as (Fossen, 2020, Chapters 6 & 8)

$$\dot{\bar{\boldsymbol{p}}} = \boldsymbol{R}(\boldsymbol{q})\boldsymbol{v} \quad (17)$$

$$\dot{\boldsymbol{q}} = \boldsymbol{T}(\boldsymbol{q})\boldsymbol{\omega} \quad (18)$$

$$\boldsymbol{M}\dot{\boldsymbol{\nu}} + \boldsymbol{C}(\boldsymbol{\nu})\boldsymbol{\nu} + \boldsymbol{d}(\boldsymbol{\nu}) + \boldsymbol{g}(\boldsymbol{p}, \boldsymbol{R}) = \boldsymbol{\tau} \quad (19)$$

where $\bar{\boldsymbol{p}} = [\boldsymbol{p}^T \; p_z]^T$ is the vehicle position, where $\boldsymbol{p}$ is the horizontal position and p_z is the vertical position. Moreover, $\boldsymbol{q}$ is a unit quaternion describing the vehicle orientation, $\boldsymbol{R}(\boldsymbol{q})$ is the proper rotation matrix associated with $\boldsymbol{q}$, and $\boldsymbol{\nu} = [\boldsymbol{v}^T \; \boldsymbol{\omega}^T]^T$ comprises the linear and angular velocities described in the vehicle frame. Furthermore, $\boldsymbol{M}$ is the vehicle inertia matrix comprising both rigid-body and hydrodynamical effects, $\boldsymbol{C}$ describes the associated Coriolis- and centripetal forces and moments acting on the vehicle, $\boldsymbol{d}$ characterizes the hydrodynamic damping forces and moments, $\boldsymbol{g}$ the hydrostatic forces and moments, and $\boldsymbol{\tau}$ the acting control forces and moments.

The ASV chosen for the simulation study is the Maritime Robotics Otter, while the AUV is the Kongsberg Maritime Remus 100. The model parameters are in both cases taken from the MSS Toolbox (Fossen and Perez, 2004).

4.2 Guidance System

The ASV and AUV are both underactuated. To facilitate effective path-following in the presence of environmental disturbances for these vehicles, we opt for an integral line-of-sight (ILOS) guidance scheme.

Given a planar continuously differentiable and regular path $\boldsymbol{\gamma}$, the path-tangential angle can be defined by

$$\vartheta(s) = \arctan_2(\gamma_2'(s), \gamma_1'(s)). \quad (20)$$

The along-track and cross-track errors are denoted ε_1 and ε_2, respectively, and are given by

$$\begin{aligned} \varepsilon_1(\boldsymbol{p}, s) &= (x - \gamma_1(s))\cos\vartheta(s) + (y - \gamma_2(s))\sin\vartheta(s), \\ \varepsilon_2(\boldsymbol{p}, s) &= (y - \gamma_2(s))\cos\vartheta(s) - (x - \gamma_1(s))\sin\vartheta(s). \end{aligned} \quad (21)$$

The ILOS guidance scheme utilized in this article is then described by (Fossen et al., 2015, Eqs. (28)-(29)).

4.3 AUV Control System

The AUV control system consists of depth and heading autopilots. Specifically, a proportional-integral (PI) controller for the depth and a proportional-integral-derivative (PID) controller for the heading.

The reference path is a circle with radius $R > 0$ centered at the point $\boldsymbol{p}_c$,

$$\boldsymbol{\gamma}(s) = \begin{bmatrix} R\cos s \\ R\sin s \end{bmatrix} - \boldsymbol{p}_c. \quad (22)$$

Furthermore, the path parameter s evolves according to

$$\dot{s} = \frac{u_d \Delta}{R\sqrt{\Delta^2 + \varepsilon_2(\boldsymbol{p}, s)^2}} + \mu\varepsilon_1(\boldsymbol{p}, s), \quad (23)$$

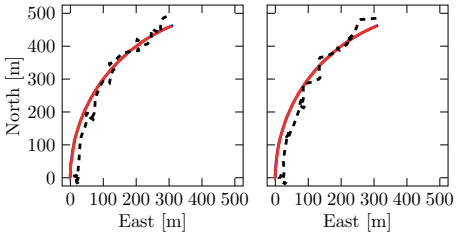

Fig. 2. Comparison of the trajectories taken with generalized variance (a), and largest eigenvalue (b). The blue line is the true trajectory of the AUV (almost entirely hidden), red is the estimated trajectory from the particle filter, and the dashed line is the ASV trajectory.

where $\mu > 0$ is a gain such that the along-track error is driven to zero, and $u_d > 0$ is the desired forward speed. The depth reference is set to 30 m, and $R = 500$ m.

4.4 ASV Control System

A planar straight-line path from the current ASV position to the target position for the current cycle is defined as

$$\boldsymbol{\gamma}(s) \coloneqq (\boldsymbol{p}_t - \boldsymbol{p}_a)s + \boldsymbol{p}_a, \tag{24}$$

where $s \in [0, 1]$. Therefore, to ensure that the ASV moves from $\boldsymbol{p}_a$ to $\boldsymbol{p}_t$ in the time interval $\Delta t = t[k] - t[k-1]$, we propose the direct *time assignment* (Skjetne et al., 2004)

$$s(t) \coloneqq \frac{t - t[k-1]}{\Delta t}, \tag{25}$$

for the path parameter, where $\boldsymbol{p}_a$ is given by (13), and $\boldsymbol{p}_t$ is given by (15), as described in Section 3. The path (24) with the time assignment (25) results in a constant nominal desired speed equal to $u_{\text{nom.}} = \|\boldsymbol{p}_t - \boldsymbol{p}_a\|/\Delta t$. We modify this nominal desired speed with a term proportional to the along-track error,

$$u_d(\boldsymbol{p}, t) \coloneqq \frac{\|\boldsymbol{p}_t - \boldsymbol{p}_a\|}{\Delta t} - c_u \varepsilon_1(\boldsymbol{p}, t). \tag{26}$$

The proportional action present in (26) ensures that the ASV will change its speed to minimize deviations from the time assignment. The gain $c_u > 0$ controls how aggressive this change of speed is. The desired speed is tracked by a PI control law.

5. RESULTS AND DISCUSSION

The proposed method has been tested in simulations, with the AUV sending an acoustic message every 4 s, after which the particle filter performs a correction step. The particle filter also uses information from the INS of the AUV, namely the heading, surge speed, and depth estimates. This information is assumed to arrive at every transmission, which is reasonable given the short distance between the two vehicles. The parameters used in the propagation model for the particle filter are$\sigma_x^2 = \sigma_y^2 = 0.16\,\text{m}^2/\text{s}^2$, $\sigma_z^2 = 0.03\,\text{m}^2/\text{s}^2$, $\sigma_\theta^2 = 4.0 \cdot 10^{-5}\,\text{rad}^2/\text{s}^2$, $\sigma_\psi^2 = 1.0 \cdot 10^{-4}\,\text{rad}^2/\text{s}^2$, $\sigma_u^2 = 2.0 \cdot 10^{-3}\,\text{m}^2/\text{s}^4$, $\sigma_{b_\theta}^2 = 5.0 \cdot 10^{-4}\,\text{rad}^2/\text{s}^4$, $\sigma_{b_\psi}^2 = 1.0 \cdot 10^{-3}\,\text{rad}^2/\text{s}^4$, $T_b = 1.0 \cdot 10^3$ s, and $\Delta t = 4.0$ s. The parameters used in the trajectory planner and particle filter are $u_{\text{nom.}} = 2.2$ m/s, $T_{\text{comms}} = 4.0$ s, $N_{\text{particles}} = 5 \cdot 10^5$, $r_1 = 16$ m, and $r_2 = 26$ m. The parameters for the estimated and true measurement models are given in Table 1.

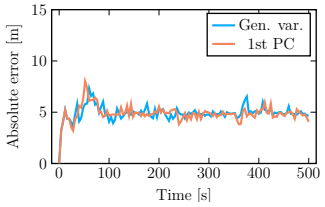

Fig. 3. Comparison of the absolute localization error by using the generalized variance for planning (blue), versus using the largest eigenvalue (red).

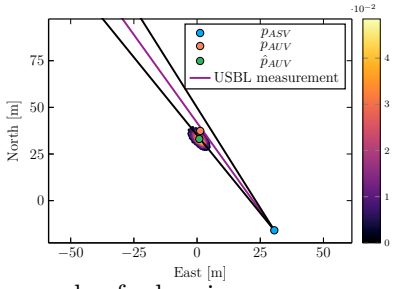

Fig. 4. An example of a bearing measurement in the NE-plane at $t = 36$ s, with the location of the ASV, AUV, and the estimated AUV position. The purple line marks the bearing measured by the USBL modem, and the black lines mark a $\pm 3°$ error bound for the bearing measurement.

First, we compare the usage of generalized variance and the largest eigenvalue for planning. Fig. 2 shows a comparison of the estimated AUV trajectories and ASV trajectories. It is clear that both evaluation metrics are able to bound the error, with it mostly hovering around 5 m. It is also apparent that the methods have similar performance, and while there seem to be more sharp turns for the ASV using the largest eigenvalue, it is not trivial to decide if this is the case, or if it just appears that way. Such an investigation is beyond the scope of this paper.

Fig. 3 shows a comparison of the absolute localization error between the two metrics. As in Fig. 2, it is clear that in terms of performance, there is not a significant difference between the two methods. This means that in the event of tracking multiple agents, one should be able to freely pick the one that makes it easiest for the planner to handle the trade-off between localization performance between the individual agents.

In Figs. 4 and 5, we show an example of the USBL measurement, particle density, as well as a comparison of $\boldsymbol{p}_{\text{AUV}}$ and $\hat{\boldsymbol{p}}_{\text{AUV}} = \frac{1}{N_{\text{particles}}} \sum_i \boldsymbol{p}_i$ at $t = 36$ s. In this case we observe that the true position of the AUV is already quite far from the center of the distribution. Fig. 6 is worse, showing that the true position of the AUV is completely outside the particle cloud. The fact that the filter underestimates the uncertainty should be investigated further in the future.

Table 1. System parameters used for measurements, with one column for the true values, and one for the estimates used in the particle filter.

Parameter	Value	Estimate	Unit
σ^2_{USBL}	$(0.01)^2$	$(0.022)^2$	$(°/\text{m})^2$
σ^2_{SOG}	0.05	0.06	$(\text{m/s})^2$
σ^2_{COG}	0.13	0.15	$(\text{rad/s})^2$
$\sigma^2_{z_{\text{meas}}}$	0.1	0.15	m^2

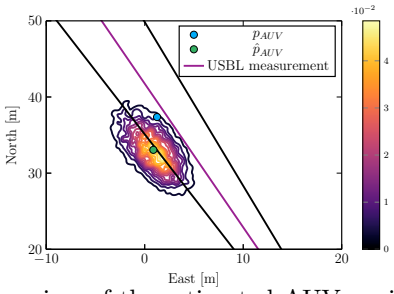

Fig. 5. Closer view of the estimated AUV position and the true AUV position at $t = 36$ s with a contour plot of the particle density. Brighter colors correspond to higher particle densities, representing a higher probability density. The purple line marks the bearing measured by the USBL modem, and the black lines mark a $\pm 3°$ error bound for the bearing measurement.

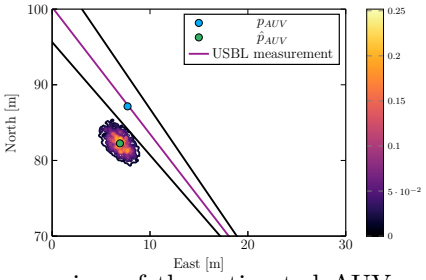

Fig. 6. Closer view of the estimated AUV position and the true AUV position at $t = 80$ s with a contour plot of the particle density. Brighter colors correspond to higher particle densities, which in turn correspond to a higher probability estimated by the filter.

6. CONCLUSIONS AND FUTURE WORK

We have derived and presented an algorithm that estimates the location of an AUV based on bearing data from a beacon located on an ASV, as well as INS data from the AUV. The presented approach estimates the state of the AUV with a particle filter, using bearing measurements from a USBL system, and data from the AUV's INS. The data from the filter is then used to plan how to strategically move the ASV to bound the localization error of the AUV. This has been demonstrated through simulations.

We observe that the effectiveness of the strategy is dependent on a surface vessel that can move significantly faster than the underwater vehicle. Further, while our approach shows promise in bounding errors, the behavior of the particle filter in predicting uncertainties may not always align with expectations, and needs further investigation.

Moving forward, we believe it is important to extend the methodology to accommodate multiple underwater vehicles and multiple beacons, generalizing the approach to multi-agent scenarios.

REFERENCES

Austin, T., Hosom, D., and Kuchta, D. (1984). Long baseline acoustic navigation - a flexible approach to custom applications. In *Proc. OCEANS 1984*.

Austin, T. (1994). The application of spread spectrum signaling techniques to underwater acoustic navigation. In *Proc. IEEE AUV'94*.

Bayat, M., Crasta, N., Aguiar, A.P., and Pascoal, A.M. (2016). Range-based underwater vehicle localization in the presence of unknown ocean currents: Theory and experiments. *IEEE Transactions on Control Systems Technology*.

Blueprint subsea (2024). Seatrac standard. URL `https://www.blueprintsubsea.com/seatrac/seatrac-standard`. Accessed: 16.02.24.

Chan, Y., Hattin, R., and Plant, J. (1978). The least squares estimation of time delay and its use in signal detection. In *Proc. IEEE ICASSP'78*.

Chitre, M.A. (2010). Path planning for cooperative underwater range-only navigation using a single beacon. *Proc. 2010 International Conference on Autonomous and Intelligent Systems*.

Crasta, N., Moreno-Salinas, D., Bayat, B., Pascoal, A.M., and Aranda, J. (2018). Range-based underwater target localization using an autonomous surface vehicle: Observability analysis. In *Proc. 2018 IEEE/ION PLANS*.

Fossen, T.I. and Perez, T. (2004). Marine systems simulator. URL `https://github.com/cybergalactic/MSS`.

Fossen, T.I. (2020). *Handbook of Marine Craft Hydrodynamics and Motion Control*. Wiley, 2nd edition.

Fossen, T.I., Pettersen, K.Y., and Galeazzi, R. (2015). Line-of-Sight Path Following for Dubins Paths With Adaptive Sideslip Compensation of Drift Forces. *IEEE Transactions on Control Systems Technology*, 23(2).

Giridhar, A. and Kumar, P.R. (2006). Distributed clock synchronization over wireless networks: Algorithms and analysis. In *Proc. IEEE CDC 2006*.

Hung, C.T., Zhang, Y.C., and Chen, C.F. (2022). Autonomous underwater acoustic localization through multiple unmanned surface vehicle. In *Proc. OCEANS 2022, Hampton Roads*.

Jaffre, F., Austin, T., Allen, B., Stokey, R., and Von Alt, C. (2005). Ultra short baseline acoustic receiver/processor. In *Proc. Europe Oceans 2005*.

Jain, R.P., Alessandretti, A., Aguiar, A.P., and de Sousa, J.B. (2018). A nonlinear model predictive control for an auv to track and estimate a moving target using range measurements. In *Proc. ROBOT'17*.

Leng, M. and Wu, Y.C. (2011). Distributed clock synchronization for wireless sensor networks using belief propagation. *IEEE Transactions on Signal Processing*, 59(11).

Moral, P.D. (1996). Nonlinear filtering: Interacting particle resolution. *Comptes Rendus de l'Académie des Sciences - Series I - Mathematics*, 2.

Moral, P.D. (1998). Measure-valued processes and interacting particle systems. Application to nonlinear filtering problems. *The Annals of Applied Probability*.

NOAA (2023). How much of the ocean has been explored? URL `https://oceanexplorer.noaa.gov/facts/explored.html`.

Skjetne, R., Fossen, T.I., and Kokotović, P.V. (2004). Robust output maneuvering for a class of nonlinear systems. *Automatica*.

Tracey, B.H. (1992). Design and testing of an acoustic ultra-short baseline navigation system. URL `https://doi.org/10.1575/1912/5495`. Master's thesis, MIT/WHOI.

Wilks, S.S. (1932). Certain generalizations in the analysis of variance. *Biometrika*, 24(3/4).